Robust 3D Bloch-Siegert based B1+ mapping using Multi-Echo General Linear Modelling

Nadège Corbin[1], Julio Acosta-Cabronero[1], Shaihan J. Malik[2], Martina F. Callaghan[1]

[1]*Wellcome Centre for Human Neuroimaging, UCL Queen Square Institute of Neurology, University College London, London, United Kingdom*

[2] *School of Biomedical Engineering & Imaging Sciences, King's College London, London, United Kingdom*

Submitted to Magnetic Resonance in Medicine on the 12th of February 2019

Running Title

MEBSS B_1^+ mapping

Keywords

B_1^+ mapping, Bloch-Siegert shift, GLM, RF spoiling, multi-echo readout, Interleaved acquisition

Corresponding author:
Nadège Corbin,
Wellcome Centre for Human Neuroimaging,
UCL Institute of Neurology,
University College London,
London, WC1N 3AR, UK
Email: n.corbin@ucl.ac.uk
Phone: +44-20-344-84383
Fax: +44-20-7813-1420

Abstract

Purpose: Quantitative MRI applications, such as mapping the T1 time of tissue, puts high demands on the accuracy and precision of transmit field (B1+) estimation. A candidate approach to satisfy these requirements exploits the difference in phase induced by the Bloch-Siegert Shift (BSS) of two acquisitions with opposite off-resonance frequency RF pulses. Interleaving these RF pulses ensures robustness to motion and scanner drifts, however, here we demonstrate that doing so also introduces a bias in the B_1^+ estimates.

Methods: We show via simulation and experiments that the amplitude of the error depends on MR pulse sequence parameters, such as TR and RF spoiling increment, but more problematically, on the intrinsic properties, T1 and T2, of the investigated tissue. To solve these problems, we present a new approach to BSS-based B_1^+ estimation that uses a multi-echo acquisition and a general linear model (GLM) to estimate the correct BSS-induced phase.

Results: In line with simulations, phantom and in-vivo experiments confirmed that the GLM-based method removed the dependency on tissue properties and pulse sequence settings. It also showed greater robustness to hardware imperfections.

Conclusion: The GLM-based method is recommended as a more accurate approach to BSS-based B1+ mapping.

Introduction

Knowledge of the spatial distribution of the radiofrequency transmit field (B_1^+) is crucial to many MRI applications. Moderate accuracy may suffice when setting transmitter gain[1] or calibrating multi-channel systems[2]. However, very high accuracy and precision are required for many quantitative MRI applications, e.g. mapping the longitudinal relaxation rate to characterise cortical myelination[3,4].

Phase-based methods may be preferred as they are theoretically insensitive to T_1 relaxation effects which often bias magnitude-based methods, especially at short TR. In the Bloch-Siegert (BS)[5] approach, an off-resonance RF pulse leads to the Bloch-Siegert frequency shift (BSS), and an associated phase accumulation, which is proportional to the square of the pulse amplitude thereby encoding the B_1^+ field. This technique performed favourably in a recent review of the accuracy, precision and practicality of a range of prominent B_1^+ mapping techniques[6], and has been shown to be less sensitive to B_0 inhomogeneities and chemical shifts[7] than other phase-based methods.

The BSS technique is flexible and can be integrated into a multitude of pulse sequences, such as 2D[5] or 3D gradient echo (GRE)[7–9], Interleaved EPI, spiral GRE[10] and spin echo[11–14] acquisitions. The BSS technique, as typically implemented, requires two acquisitions with opposite off-resonance frequencies. By subtracting the two phase images, the BSS effect is enhanced and unrelated phase components are removed, e.g. phase accumulated across echo time (TE) due to B_0 inhomogeneity or chemical shifts, due to eddy currents, or any initial phase due to the transmitting and receiving coils. This subtraction also has the advantage of removing the effect of B_0 inhomogeneity on the BSS, up to first order[5]. These two acquisitions can either be played out sequentially or by interleaving the opposite, off-resonance frequencies. Previous reports have shown the interleaved approach to be more robust to motion[15] and magnetic field drift[8].

In this work, we focus on a 3D spoiled GRE implementation and demonstrate, through both simulations and experiments, that alternating the sign of the off-resonance frequency from shot to shot in an interleaved fashion disturbs the steady-state and introduces an additional phase difference between the two acquisitions, especially at short TR. We show that this additional phase difference leads to bias in the B_1^+ map that depends on the relaxation parameters of the studied tissue, the specifics of the RF spoiling regime and the actual B_1^+ amplitude. We additionally propose and validate a modified BSS-based approach that removes these dependencies. The solution consists of a multi-echo acquisition in which several echoes are acquired before and after the BS pulse and modelling the phase evolution with a General Linear Model (GLM). We demonstrate that this GLM-based approach to isolating the BSS phase allows the interleaved approach to be used without introducing any error, extending the acquisition time, increasing the SAR or reducing the sensitivity.

Theory

In line with [5], and as detailed in the supplementary information (S.I.1), the BS phase introduced by an RF pulse with peak amplitude B_1^p and normalised shape B_1^{norm}, is proportional to the square of the peak pulse amplitude:

$$\Phi_{BSS} = \left(B_1^p\right)^2 \int_0^T \left(\gamma\, B_1^{norm}(t)\right)^2 * \left(\left[\frac{1}{2\omega_{off}} - \frac{\Delta\omega_{B_0}}{2\omega_{off}^2}\right] + O\left(\Delta\omega_{B_0}^2\right) \right) dt \qquad (1)$$

ω_{off} is the off-resonance frequency of the pulse and $\Delta\omega_{B_0}$ is the local field inhomogeneity, both in Hz.

The classic method: isolating the BSS phase by subtraction

The classic approach to BSS-based B_1^+ mapping consists of acquiring two datasets with BS pulses of opposite off-resonance frequency (i.e. $+\omega_{off}$ and $-\omega_{off}$). The phase difference between these is:

$$\Phi_{BSS_{Diff}} = \left(B_1^p\right)^2 \int_0^T \left(\gamma\, B_1^{norm}(t)\right)^2 * \left(\left[\frac{1}{2\omega_{off}} - \frac{\Delta\omega_{B_0}}{2\omega_{off}^2}\right] - \left[-\frac{1}{2\omega_{off}} - \frac{\Delta\omega_{B_0}}{2\omega_{off}^2}\right] + O\left(\Delta\omega_{B_0}^2\right) \right) dt \quad (2)$$

Since the first order terms that depend on $\Delta\omega_{B_0}$ cancel, this expression simplifies to:

$$\Phi_{BSS_{Diff}} = \left(B_1^p\right)^2 \int_0^T \frac{\left(\gamma\, B_1^{norm}(t)\right)^2}{\omega_{off}} dt + O\left(\Delta\omega_{B_0}^2\right) \quad (3)$$

Previously this subtraction was assumed to also remove any phase accumulated from other sources, such as eddy-currents, transmit/receive-related phase offsets, chemical shifts and local B_0 inhomogeneities. However, crucially, this is only true if the additional phase components are identical for each of the off-resonance frequencies. If this assumption is violated, the B_1^+ estimate will be erroneous.

The GLM method: isolating the BSS phase by modelling a multi-echo acquisition

We propose an alternative to the classic BSS approach that computes accurate B_1^+ maps even if conditions vary between the two off-resonance frequency acquisitions. This approach relies on two novel features:

A dual-offset multi-echo sequence:

In the modified BSS-based B_1^+ mapping sequence (Fig.1), multiple echoes are acquired after one excitation pulse. Two echoes, prior to the BS pulse, have previously been used[16] to concurrently compute the B_0 inhomogeneity, whereas here multiple echoes are acquired before and after the BS pulse. As in the classic, a second acquisition is performed with the opposite off-resonance frequency, either sequentially or interleaved.

A general linear model:

The GLM approach models the phase data, Y, as multiple linear sources of phase accumulation over time: $Y = X\beta + \epsilon$.

Each row of the model matrix X, corresponds to a single echo. The following explanatory variables model distinct sources of phase evolution:

X_{BSS}: Models the phase accumulated due to the BS pulse, specifically the first term of the sum in Eq.1 (only). This phase should only be present after the BS pulse, and should change sign with the off-resonance frequency. The regressor consists of zeros for echoes before the BS pulse and either 1 or -1 afterwards depending on the BS pulse frequency.

$X_{\Delta\omega_{B_0}}$: Models the phase accumulated due to local B_0 inhomogeneities. Regressor values are echo times.

$X_{Odd/Even}$: Models the phase difference between odd and even echoes due to eddy currents generated by the bipolar readout gradients. $X_{Odd/Even}$ is 1 for odd echoes and -1 for even echoes.

X_{Offset^+} and X_{Offset^-}: Models the initial phase offset of the acquisitions with positive and negative off-resonance frequencies respectively. X_{Offset^+} is 1 for echoes after a BS pulse with positive off-resonance frequency, and 0 for echoes after a BS pulse with negative off-resonance frequency; vice versa for X_{Offset^-}.

$X_{SameSign}$: Models phase consistently accumulated during the BS pulse and the crushers, regardless of the sign of the BS pulse's off-resonance frequency. This includes the second term in Eq. 1 and, for example, any phase due to eddy currents generated by the crushers.

The parameters β constitute the regression coefficients and are estimated voxel-wise via the Weighted Least Square approach: $\hat{\beta} = (X^T W X)^{-1} X^T W Y$. W is a diagonal weighting matrix in which the weights are the magnitude of the echoes. β_{BSS}, the parameter of interest, is considered an estimate of Φ_{BSS}. ϵ is an error term.

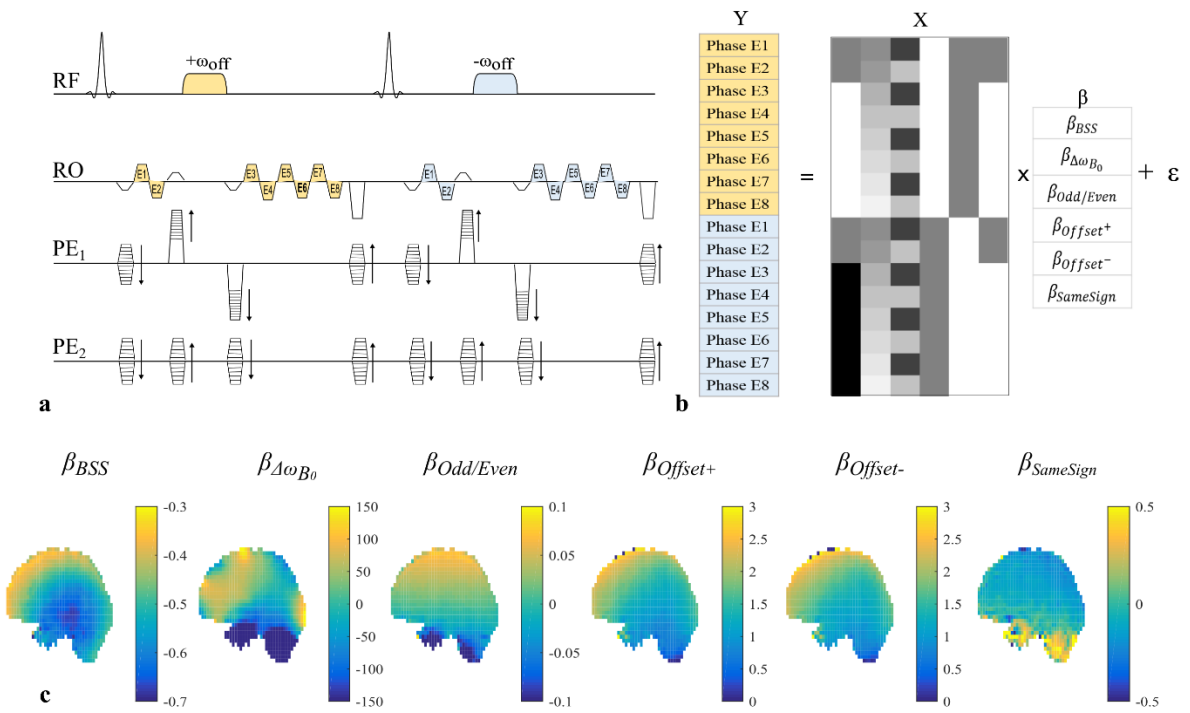

Figure 1: *The sequence diagram of the modified 3D multi-echo gradient echo for BSS-based mapping is illustrated in (a). Two echoes are acquired prior to, and six echoes after, the Bloch-Siegert pulse, which is flanked by crushers in one phase-encoding direction (PE_1) to destroy any inadvertent on-resonance excitation and minimize dependence on excitation flip angle. The gradients on each axis are balanced prior to the BS pulse. In this example, 8 echoes are acquired for each off-resonance frequency with two before and 6 after the BS pulse, resulting in a total of 16 phase images from which the B1+ efficiency is mapped. A GLM is used to model the phase variation across echo times (b). Typical maps of model coefficients obtained in vivo (c) exemplify the phase accrued due to the Bloch-Siegert shift (β_{BSS}), B0 field inhomogeneity, $\left(\beta_{\Delta\omega_{B_0}}\right)$, alternating readout (RO) polarity, $\left(\beta_{Odd/Even}\right)$, initial phase offsets specific to the off-resonance frequency of the pulse, $\left(\beta_{Offset^+}, \beta_{Offset^-}\right)$, and any additional phase due to the presence of the block of crushers and the BS pulse that is independent of the sign of the off-resonance frequency of the pulse, $(\beta_{SameSign})$.*

Methods

Numerical simulations

Simulations were used to evaluate the difference, both before and after the BS pulse, between two acquisitions with opposite off-resonance frequencies. Any difference present at this point would introduce an error in B_1^+ estimated with the classic method. A typical GRE acquisition was simulated by a series of matrix operations (described in supplementary information S.I.2). Several configurations were investigated:

Effect of RF Spoiling increment

RF spoiling modifies the phase of the excitation pulse and the BS pulse (ϕ) so that the phase difference between successive TR periods increases linearly by a constant amount $\phi_{BaseInc}$.
The impact of the RF spoiling increment was investigated by changing $\phi_{BaseInc}$ from 0 to 180 degrees in 10 degree steps. A phase increment of 0 corresponds to no RF spoiling (i.e. $\phi = 0$ for all pulses).

Sequential or Interleaved

For an interleaved acquisition, the sign of ω_{off} was alternated between successive BS pulses. For sequential acquisitions, the sign was switched after half the total number of pulses $\left(\frac{N_{exc}}{2}\right)$, at which point RF spoiling was also reset.

Effect of TR, T_1, T_2 and B_1^p

Extreme values were used to test the impact of sequence parameters, $B_1^p \in [8,11]\ \mu T$ and $TR \in [30,100]\ ms$, and relaxation parameters, $T_1 \in [550,1350]\ ms$ and $T_2 \in [70, 100]\ ms$ on the B_1^+ estimate.

The estimated B_1^+ amplitude was simulated as follows:

$$B_1^p = \sqrt{\frac{\Phi_{BSS}}{\int_0^T \frac{\left(\gamma\, B_1^{norm}(t)\right)^2}{2\,\omega_{off}} dt}} \qquad (4)$$

For the Classic method, Φ_{BSS} was taken to be half the phase difference after the BS pulse of the acquisitions with opposite off-resonance frequency, and termed $\Phi_{BSS}^{Classic}$ (SI2.1).

For the GLM method, Φ_{BSS} was taken to be the mean absolute phase accrued during the BS pulses of these, and termed Φ_{BSS}^{GLM} (SI2.2).

MRI measurements

MR pulse sequence

Measurements were performed at 3T using a body coil for transmission and a 32-channel head coil for signal reception using an in-house MR pulse sequence (Fig.1).

A Fermi pulse of duration T=2ms imparted the BSS after the second echo. Acquiring two echoes before the BS pulse served to minimize the correlation of the X_{BSS} regressor with other regressors while maintaining a reasonable TE for the echo after the BS pulse. The encoding gradients on all axes were balanced immediately prior to the BS pulse, to ensure the same dephasing state for the magnetisation across TRs, and played again just after. Crusher gradients were played out either side of the BS pulse, concurrently with the balancing/phase-encoding gradients (on PE_1), to crush any undesired on-resonance excitation and to minimise any dependence on the excitation flip angle. As demonstrated by[16], perfect dephasing of the transverse magnetization before the BS pulse is required to fully remove any such dependence. Therefore a relatively large crusher moment[17], designed to generate a theoretical dephasing of 6π rad across a voxel, was used.

For sequential acquisitions the positive and negative off-resonance frequency pulses were played out in consecutive blocks. In the interleaved case the off-resonance frequency was alternated across successive TR periods. To achieve steady state, 200 dummy cycles were executed before each block in the sequential case, 400 cycles were used at the outset of the interleaved case (to match acquisition times), and in both cases a spoiler gradient, set to reach a dephasing of 6π at the end of the TR, was applied in the readout direction after the last echo. The RF spoiling was reset at the end of the first block in the sequential case.

The same sequence reduced to only the excitation pulse (i.e. no BS pulse), data acquisitions, and spoiler gradient was used to measure the phase of the Free Induction Decay (FID) signal.

B_1^+ map estimation

All data, including B_1^+ maps, were reconstructed in real time using in-house code implemented in Gadgetron [18]. An apodizing filter was applied to the raw k-space data along each dimension to minimize ringing artefacts. After Fourier transformation the images were adaptively combined across coil elements[19].

Two B_1^+ maps were computed for each dataset using the Classic and GLM methods respectively. For the Classic method, the phase of the third echoes, which were acquired after the positive and negative off-resonance frequency BS pulses, were subtracted to estimate the BSS phase: $\Phi_{BSS} = \frac{\Phi_{Diff}}{2}$. For the GLM method, the phase images for each off-resonance frequency were temporally unwrapped, by spatially unwrapping the differences between successive echo pairs[20], and cumulatively adding these to the phase of the first echo. The phase images were subsequently used to estimate the parameters of the GLM (Fig.1). The BSS phase Φ_{BSS} was captured by the first regressor X_{BSS} of the model matrix such that $\Phi_{BSS} = \beta_{BSS}$.

For both methods, B_1^p was computed on a voxel-wise basis using Eq.4.

Phantom experiments

B_1^+ maps were acquired on an FBIRN agar phantom [21]. Experiments 1 and 2 used both the Classic and GLM processing methods to construct B_1^+ maps. B_1^+ errors were quantified as the percent difference of the estimated B_1^+ with respect to a reference B_1^+ map.

<u>Phantom Experiment 1: Comparing processing approaches</u>

This experiment probed the impact of the processing method as a function of the RF spoiling increment, $\phi_{BaseInc} \in [0;\ 10;\ 50;\ 60;\ 70;\ 90;\ 110;\ 120;\ 130;\ 160;\ 170;\ 180]$). The interleaved acquisition scheme was used for all scans. B_1^+ maps were reconstructed with the Classic and GLM methods. The voxel-wise difference between the two B_1^+ maps (relative to the GLM method) was computed, and summarised by the mean and standard deviation across the phantom. A TR of 30 ms was used.

<u>Phantom Experiment 2: Comparing sequential and interleaved approaches</u>

A reference B_1^+ map was obtained, via the Classic method, using a sequential acquisition with $\phi_{BaseInc} = 90°$. Four interleaved acquisitions were performed with:

No RF spoiling, TR=35ms

$\phi_{BaseInc} = 137°$, TR=35ms

$\phi_{BaseInc} = 90°$, TR=35ms

$\phi_{BaseInc} = 90°$, TR=100ms

B_1^+ maps were created using both Classic and GLM methods and compared to the reference map. Histograms of the relative difference in B_1^+ estimates were calculated for each RF spoiling condition and processing method.

<u>Phantom Experiment 3: Assessing phase stability</u>

The FID phase was measured under different conditions:

With and without RF spoiling,

Short and long TR (30 and 100 ms)

Small and large excitation flip angle (6 and 15 degrees)

Three different RF spoiling increments (90, 117 and 137 degrees).

Although no BS pulse was played out in these experiments, the time series were processed as if an interleaved acquisitions scheme had been adopted.

In vivo experiments

In vivo Experiment 1

Three healthy participants (2 males, 28-40 years) were scanned on the Prisma scanner. Five datasets were acquired per participant, with TR=35ms unless otherwise stated:

1. Interleaved, with $\phi_{BaseInc} = 137°$ and TR=100ms. This produced the reference B_1^+ map.

2. Interleaved without RF spoiling

3. Interleaved with $\phi_{BaseInc} = 137°$

4. Interleaved with $\phi_{BaseInc} = 90°$

5. Sequentially with $\phi_{BaseInc} = 137°$

Two B_1^+ maps were estimated for each scan using the Classic and GLM methods respectively. The percent difference in B_1^+ was calculated with respect to the reference map for the same processing method. To compare processing methods, the percent difference between the two B_1^+ maps derived from the reference acquisition was also computed, with respect to that obtained with the Classic method.

In vivo Experiment 2

The experiments carried out in phantom experiment 3 were repeated *in vivo*.

Table 1 lists sequence parameters of all experiments. Phantom experiments 1 and 3 were performed on a Trio (Siemens, Erlangen Germany). Phantom experiments 2 and 3, and the *in vivo* experiments, were performed on a Siemens Prisma.

$\boldsymbol{TR}$	Repetition time	30 ms for Phantom experiment 1 35 ms for Phantom experiment 2; 100 ms for the reference 35 ms for In vivo experiment 1; 100 ms for the reference
$\boldsymbol{TE}$	Echo times	[2.38 4.68 11.42 13.72 16.02 18.32 20.62 22.92] ms (Phantom experiment 2 and in vivo experiment 1) [2.23 4.63 11.09 13.49 15.89 18.29 20.69 23.09] ms (Phantom experiment 1)
$\boldsymbol{\omega_{off}}$	Off-resonance frequency of the BS pulse	2 kHz
$\boldsymbol{\alpha_{BS}}$	Flip angle of the BS pulse	260 °
$\boldsymbol{T}$	Duration of the BS pulse	2 ms
$\boldsymbol{\alpha}$	Excitation flip angle	15 °

$\boldsymbol{\phi_{BaseInc}}$	Increment of the RF spoiling	[0° 10° 50° 60° 70° 90° 110° 120° 130° 160° 170° 180°] for Phantom experiment 1 [0° 90° 137°] for Phantom experiment 2 [0° 90° 137°] for *in vivo* experiment 1
$\boldsymbol{\Omega_1^{max}}$	Crusher gradient dephasing moment	6 π rad
$\boldsymbol{\Omega_2^{max}}$	Spoiling moment per TR	6 π rad
	Field of view	256 × 224 x 192 mm^2
	Acquisition matrix	56 × 64 x 48
	Voxel size	4x4x4 mm^3

Table 1: *List of the parameters of the phantom and in vivo acquisitions*

Results

Numerical simulations

Effect of acquisition order and RF spoiling

For sequential acquisition ordering, once steady-state was reached for each off-resonance frequency blocks (Fig.2 a), the phase difference between these was zero before the BS pulse (Fig.2 c). It was non-zero after the BS pulse (Fig.2 e) since it contained the BSS phase. However, this BSS phase estimate remained constant over time and was independent of the RF spoiling condition.

For interleaved acquisitions, the phase before the BS pulse varied from pulse to pulse regardless of pulse number (Fig.2 b). This temporal variance caused a non-zero phase difference between the interleaved acquisitions with opposite BS pulse frequencies, both before (Fig.2 d) and after (Fig.2 f) the BS pulse. Furthermore, the phase difference after the BS pulse, i.e. the estimate of the BSS phase, differed from the phase difference obtained with the sequential approach and depended strongly on the RF spoiling conditions.

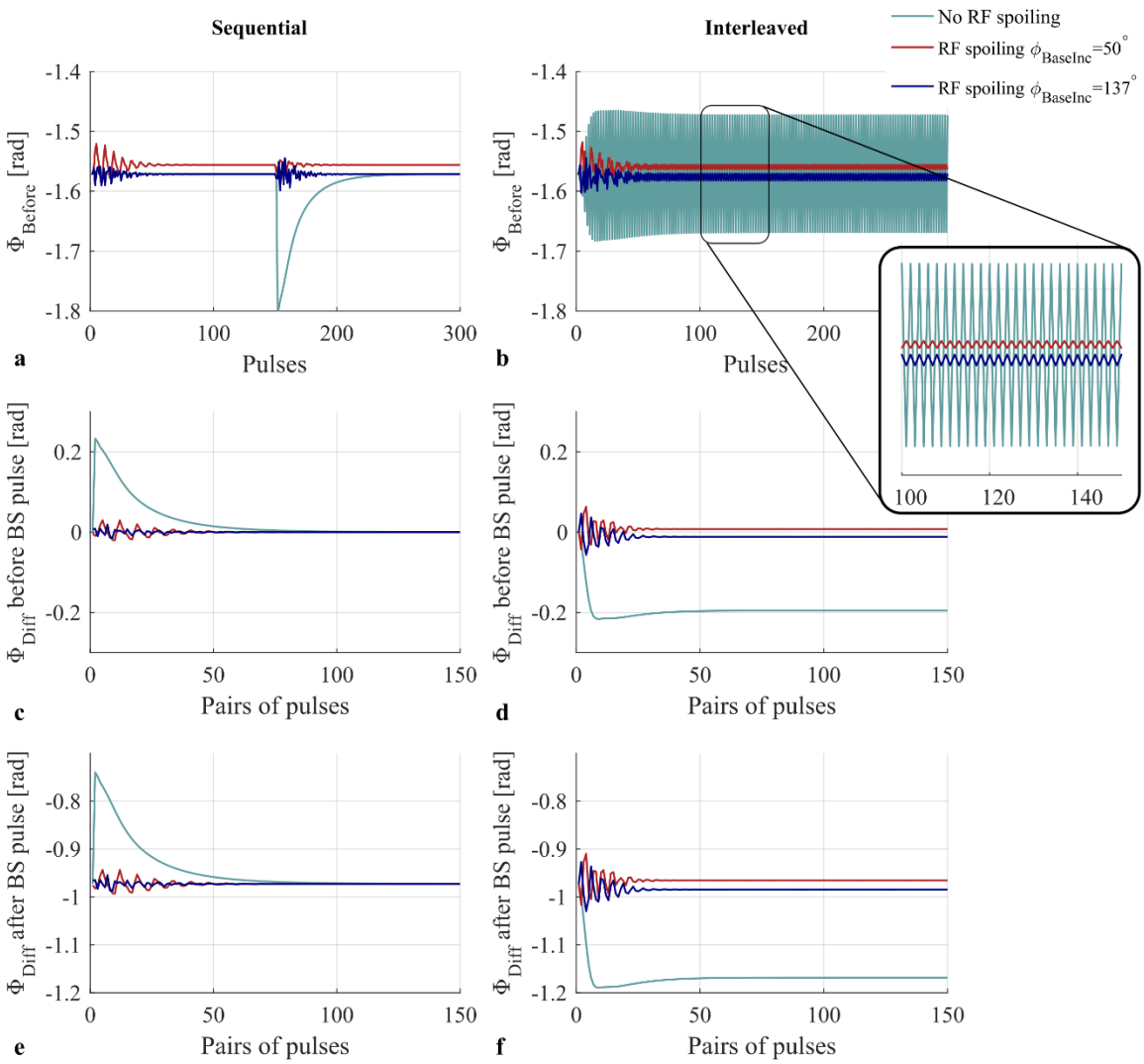

Figure 2: *Numerical simulation results. Phase acquired prior to the BS pulse in case of sequential acquisitions (a) or interleaved acquisitions (b), in the presence (red curve) or not (green) of RF spoiling* ($\Phi_{BaseInc} = 137°$). *Phase difference prior to the pulses of the two acquisitions with opposite frequencies (c-d) and phase difference after the BS pulse (e-f).*

Effect of RF spoiling increment

The error in the BSS phase resulting from simulating an interleaved acquisition and using the Classic method depended strongly on the RF spoiling increment used (Fig.3). The greatest errors were predicted for phase increments of 0° (equivalent to no RF spoiling) and 180°. Large errors were also predicted for phase increments of 60° and 120° whereas no error was predicted at 90°.

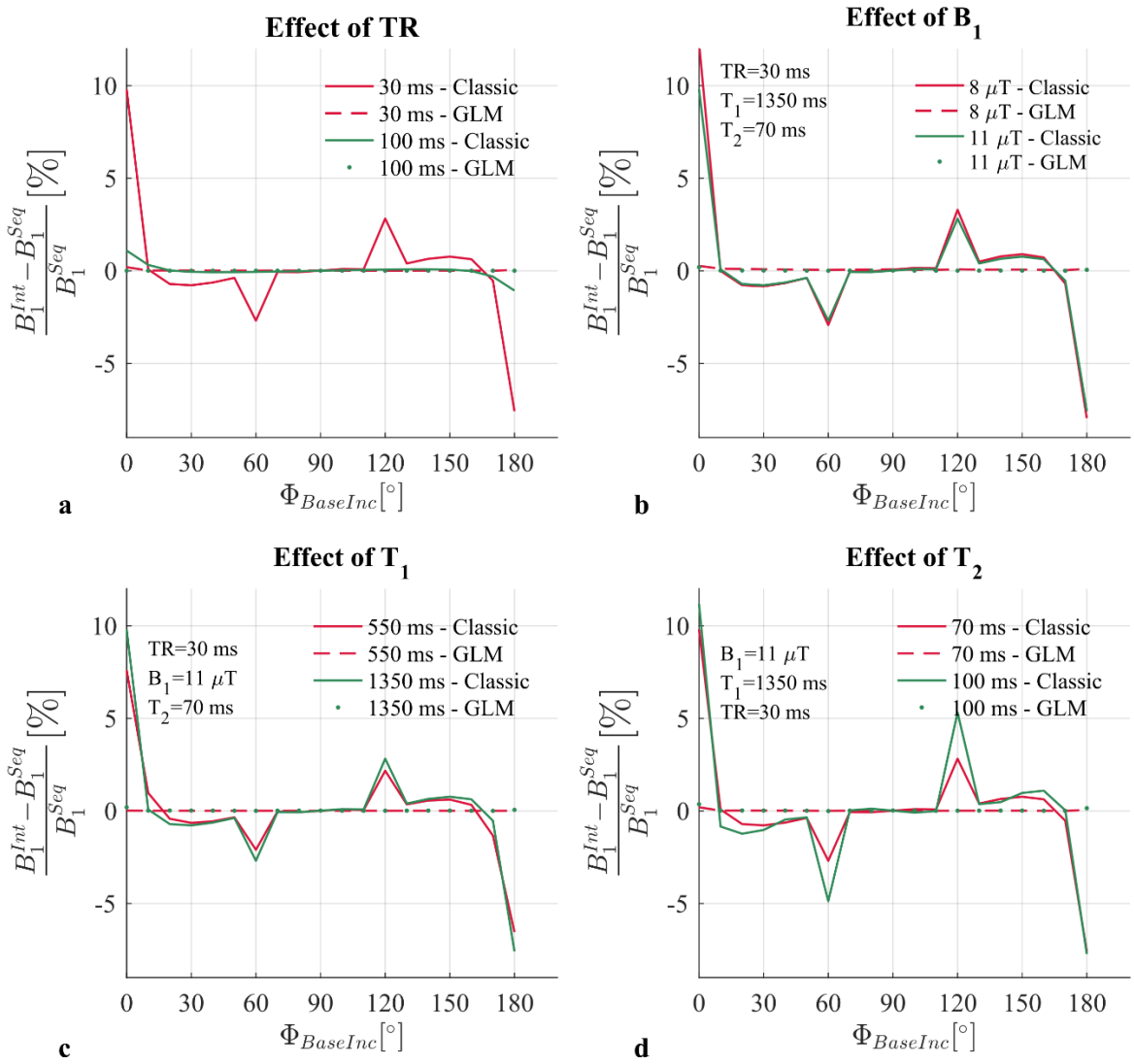

Figure 3: *Numerical simulation results. Relative error of the estimate of B_1^+ obtained with interleaved acquisitions B_1^{Int} with respect to the estimated B_1^+ obtained with sequential acquisitions B_1^{Seq}. B_1^{Int} is computed in two ways, the Classic method solid lines, and the GLM method (Eq.4), dashed and dotted lines. B_1^{Seq} is only computed with the Classic method. The error is observed over a large range of RF spoiling increment ($\Phi_{BaseInc} \in [0:10:180]$), for two TR values (a), two B_1^+ values (b), two T_1 values (c) and two T_2 values (d).*

Effect of TR, B_1^+, T_2 and T_1.

Increasing TR greatly reduced the predicted error in Φ_{BSS} (Fig.3 a). Longer T_1 times led to larger predicted errors, but less impact than TR, (Fig.3 c). Similarly, longer T_2 times predicted larger errors (Fig.3 d), especially with phase increments of 60 and 120° where the predicted error was already large.

The amplitude of the BS pulse also had a small impact whereby the *relative* error was predicted to be lower for higher amplitude pulses (Fig.3 b). Note that in this case B_1^+ also increases, so while the predicted relative error decreased, the absolute error is actually increased.

Impact of GLM method for BSS estimation

The numerical simulations predicted that these errors were removed by using the GLM approach. As a result, the derived B_1^+ estimates were predicted to be stable and agree with the B_1^+ estimated from the sequential case using the Classic method. This was the case regardless of the RF spoiling conditions, TR, T_1, T_2 or BS pulse amplitude.

Phantom experiments

Phantom Experiment 1: Comparing processing approaches

With RF spoiling increments of 0 and 180°, the B_1^+ estimates were very different depending on the processing method used (Fig.4), but agreed when the RF spoiling increment was 90°. Two further peaks in the discrepancy were observed with RF spoiling increments of 60° and 120°. The difference observed without RF spoiling ($\Phi_{BaseInc} = 0°$) was 3.6%.

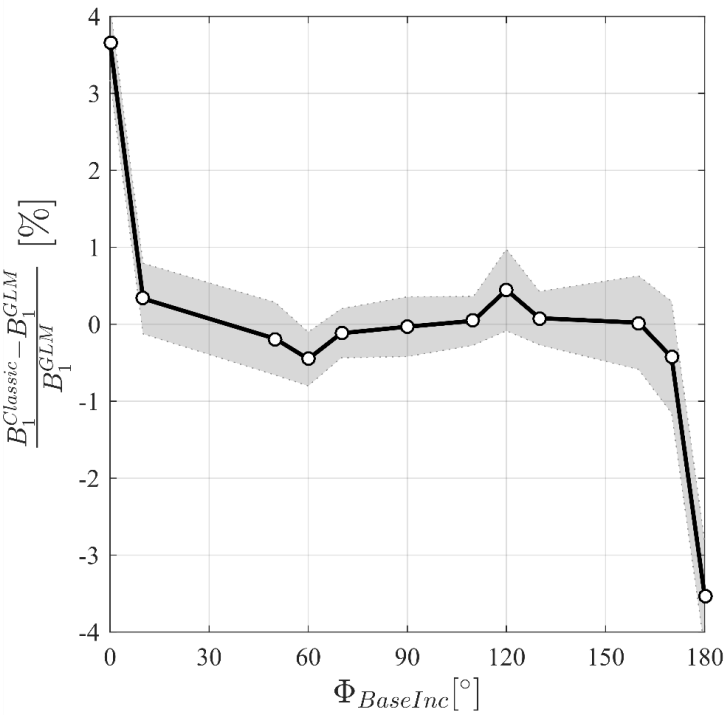

Figure 4: *Phantom experiment performed on the Trio scanner. Relative difference of the B_1^+ map obtained with the Classic method $B_1^{Classic}$, with respect to the B_1^+ map reconstructed with the GLM method. One cross is the average difference across the phantom. B_1^+ map are obtained with interleaved acquisitions and repeated over a range of RF spoiling increment $\Phi_{BaseInc} = [0\ 10\ 50\ 60\ 70\ 90\ 110\ 120\ 130\ 160\ 170\ 180]°$.*

<u>Phantom Experiment 2: Comparing sequential and interleaved approaches</u>

B_1^+ maps estimated using the Classic method from interleaved data and sequential data (the reference case) did not agree. The largest bias was observed with no RF spoiling (median (IQR) of 2.92% (0.45), Fig.5 a) and was greatly reduced by RF spoiling (-0.25% (0.42) with $\phi_{BaseInc} = 90°$ and -0.02% (0.98) with $\phi_{BaseInc} = 137°$). Negligible bias was observed with a longer TR of 100ms (0.05% (0.26)).

All biases relative to the sequential case were removed when the GLM method was used to process the same interleaved data (Fig.5 b; 0.01% (0.34), -0.01% (0.39) and -0.01% (0.48) for no RF spoiling and RF spoiling with $\phi_{BaseInc} = 90°$ and $\phi_{BaseInc} = 137°$ respectively).

On this scanner (Prisma), it was also observed that the Classic method increased the variance of the relative B_1^+ error at short TR using RF spoiling, especially for $\phi_{BaseInc} = 137°$ (Fig.5 a). A small bias was also observed for $\phi_{BaseInc} = 90°$. However, the B_1^+ maps reconstructed by the GLM method were insensitive to these issues (Fig.5 b).

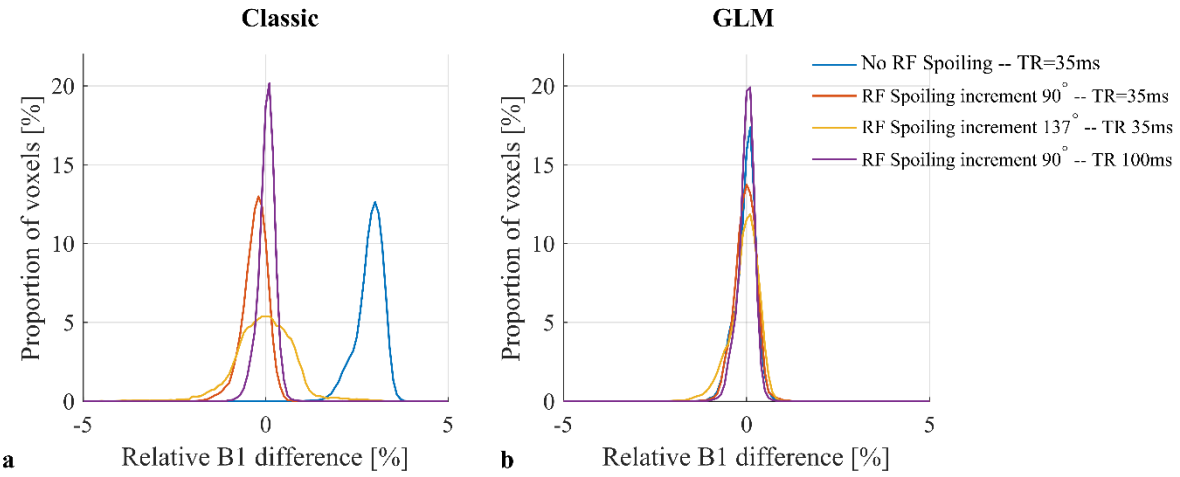

Figure 5: *Histograms of the difference in B_1^+ measured in a phantom with an interleaved acquisition scheme relative to the reference B_1^+ map acquired with a sequential acquisition and processed using the Classic method. The B_1^+ maps were calculated using either the Classic (a) or GLM (b) method. The data were acquired with a short TR (35ms) without (blue) or with RF spoiling ($\Phi_{BaseInc} = 137°$ $(yellow)$ and $\Phi_{BaseInc} = 90°$ (red)), or a long TR (100ms) and RF spoiling ($\Phi_{BaseInc} = 90°$) $(purple)$. The reference B_1^+ map, with respect to which the error was calculated, was acquired with sequential ordering and RF spoiling ($\Phi_{BaseInc} = 90°$) and processed using the Classic method.*

Phantom Experiment 3: Assessment of phase stability

Without RF spoiling, both scanner platforms showed stable phase over time. However, appreciable temporal phase variations were observed when RF spoiling was used on the Prisma scanner (Fig.6 b-g, middle column). The amplitude of this variation was reduced when the excitation flip angle was decreased (Fig.6 f) or the TR was increased (Fig.6 g). The pattern of variation was highly reproducible across repetitions (Fig.6 b, c) and depended on the particular RF spoiling increment used (Fig.6 c, d, e). In contrast, the phase of the FID measured on the Trio scanner was temporally stable regardless of RF spoiling conditions.

	RF Spoiling Increment $\Phi_{BaseInc}$ [°]	TR [ms]	Excitation flip angle α [°]
a	0	35	15
b	137	35	15
c	137	35	15
d	90	35	15
e	117	35	15
f	137	35	6
g	137	100	15

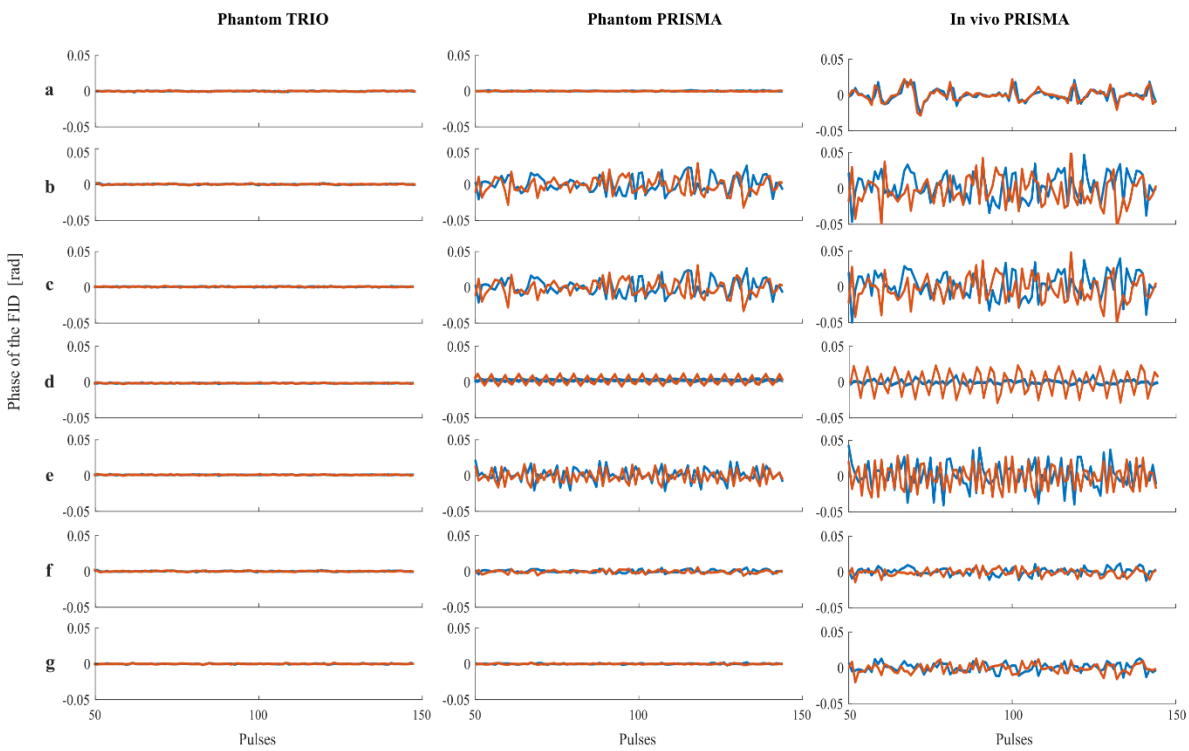

Figure 6: *FID phase of the two interleaves acquired on phantom (left and middle columns) and in vivo (right column) with the Trio scanner (left column) and the Prisma scanner (middle and right column). The BS pulse and all the gradients apart from the spoiler were turned off. Several configurations listed in the table were investigated. The phase of the two interleaves are different depending on the scanner used when RF spoiling is turned on. On the Prisma, a phase variation is observed with a pattern of variation reproducible across runs (b versus c) and the same pattern is observed in vivo and on phantom. The pattern depends on the RF spoiling increment (c versus d versus e) . The amplitude decreases as TR increases (b versus g) or the flip angle decreases (b versus f).Without RF spoiling a phase variation is observed in vivo, likely due to physiological sources.*

In vivo experiments

In vivo Experiment 1

The reference acquisition with interleaved ordering, a longer TR of 100ms and an RF spoiling increment of $\phi_{BaseInc} = 137°$ produced consistent B_1^+ maps from the Classic and GLM methods (Fig.7 c, f, i). The median (IQR) differences relative to the GLM method were: -0.05% (0.95), -0.02% (0.80) and 0.12% (0.77) for participants 1, 2 and 3, respectively.

Large bias was seen with respect to this reference when B_1^+ maps were estimated from interleaved data, acquired without RF spoiling, using the Classic method (Fig.7 a, d, g). Qualitatively, the bias was highly visible in the B_1^+ maps (Fig.8 a) following anatomical detail, and was greatest in the ventricles with long T_1 and T_2. In the difference map, strong bias was visible along the cortical ribbon (Fig.8 b). Median (IQR) differences were 4.57% (2.70), 4.65% (2.73), 5.21% (3.07) for participants 1, 2 and 3, respectively. These biases were greatly reduced when the data were processed using the GLM method: -0.06% (1.36), -0.04% (1.55) and 0.61% (1.64), respectively (Fig.7 b, e, h; Fig.8 c, d).

The bias was greatly reduced when RF spoiling was used ($\Phi_{BaseInc} \in [90°, 137°]$) and never exceeded 0.78% and 0.51% when estimated using the Classic and GLM methods respectively (Fig.7, yellow and purple curves). The IQR was slightly decreased by the GLM method for participants 2 and 3, but not for participant 1 for whom the variance was already low with the Classic method.

High variability in B_1^+ bias was observed when the sequential acquisition ordering was used (Fig.7, blue curves) and artefacts were visible in the B_1^+ and difference maps (Fig.8 a-d). This was the case regardless of the processing approach.

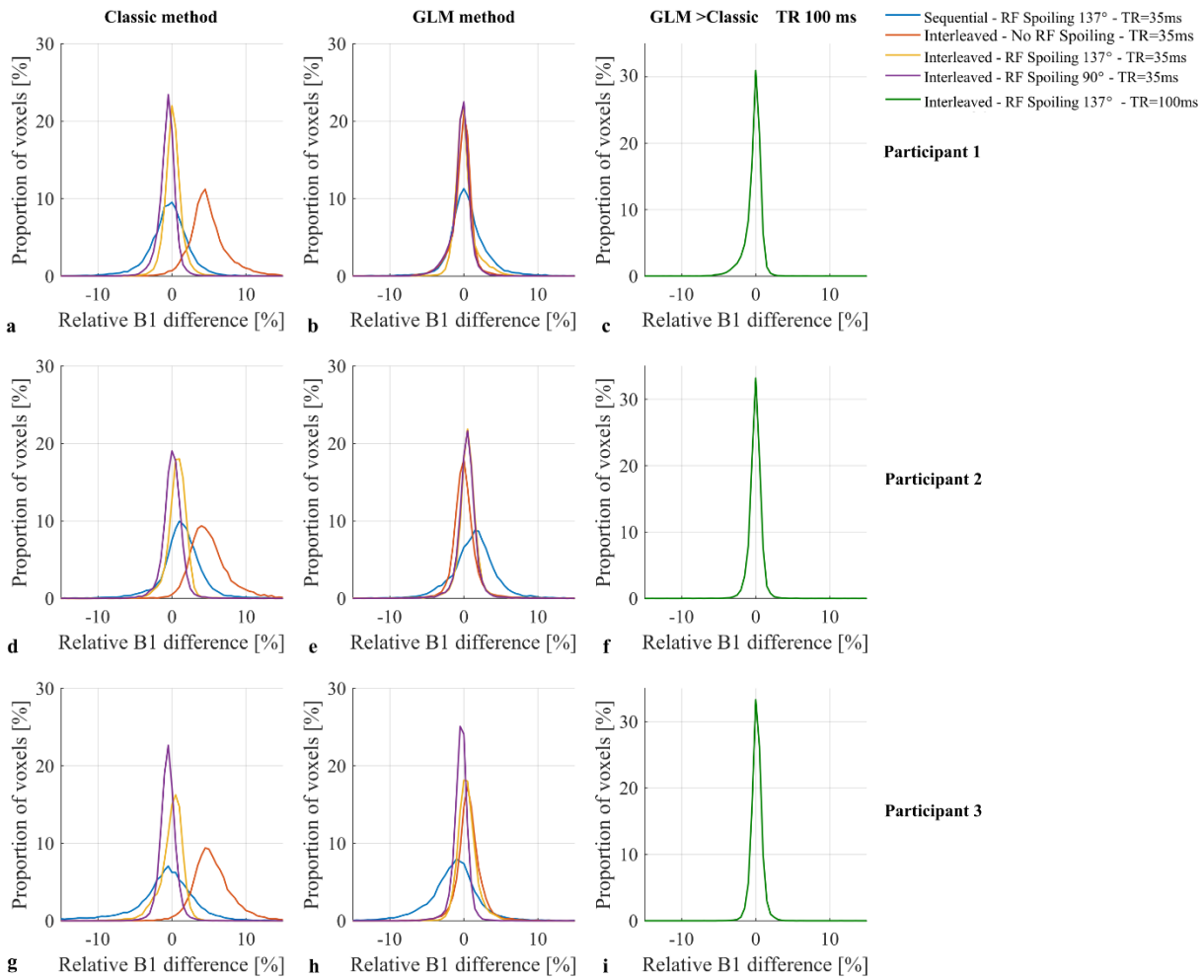

Figure 7: *Histograms of the difference in B_1^+ relative to the reference B_1^+ map acquired in vivo with RF spoiling ($\Phi_{BaseInc} = 137°$) with a TR of 100ms, in interleaved order. The B_1 maps are either calculated with the*

classic method (a-d-g) or the GLM method (b-e-h). Percentage difference between the reference B_1^+ maps computed with the GLM and the Classic methods (c-f-i). Each row corresponds to a different participant.

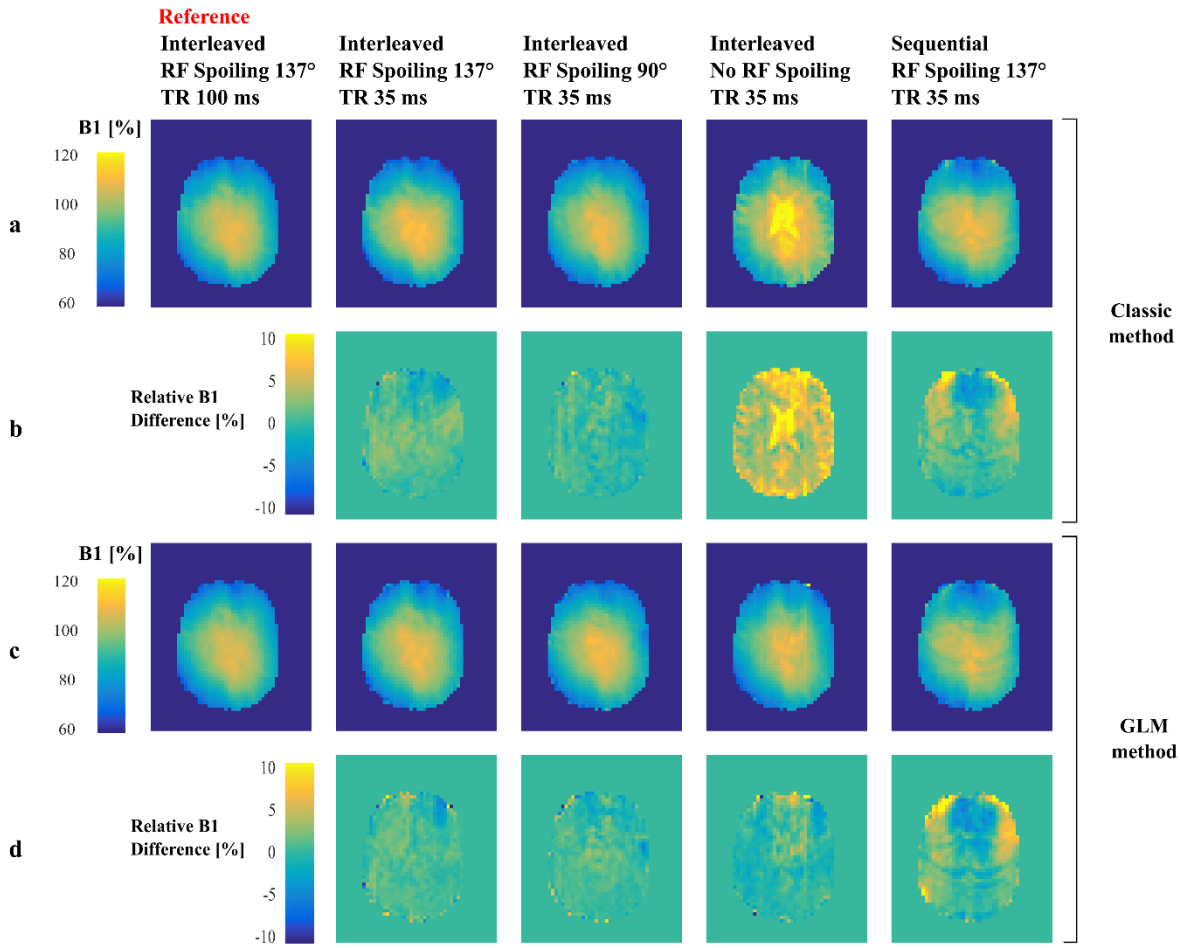

Figure 8: *B_1^+ maps of one slice obtained on Participant 2 with the Classic (a) and the GLM approach (c) with 5 different protocols. Maps of the relative difference of each B_1^+ map with the reference maps computed with the same method: Classic (b) or GLM (d) approach.*

<u>*In vivo* Experiment 2:</u>

The phase of the FID signal measured *in vivo* on the Prisma scanner platform showed the *same pattern* of variation as the corresponding phantom experiments (Fig.6, right column). With RF spoiling, the amplitude of the variation observed was of the same order as the phase observed without RF spoiling (Fig.6 a). The case of no RF spoiling is likely to be indicative of physiologically-driven phase variation, since no such variation was seen in the phantom experiments.

Discussion

Efficient methods for mapping the B_1^+ transmit field with high accuracy and precision are prerequisite for demanding MRI applications, such as the quantification of the longitudinal relaxation rate[3]. Biases in B_1^+ estimates may underlie inter-site differences in relaxation rates[22] while uncertainty in the

estimates will lower reproducibility[4]. B_1^+ mapping based on the phase accrued due to the Bloch-Siegert shift has been reported to be an efficient technique for accurately estimating the spatial distribution of B_1^+ when compared to other magnitude or phase-based techniques[6,23].

Our numerical simulations indicate that the sequential approach for acquiring the necessary BSS data will deliver a bias-free estimate of the B_1^+ field. However, in agreement with previous reports[15,8], our *in vivo* experiments show that this approach is sensitive to phase perturbations over time such as those causes by motion and scanner drifts. The resulting B_1^+ maps had visible artefacts and large biases (Fig.8, right column). The greater robustness of the interleaved acquisition scheme has led to its adoption in more recent work using this technique[9,24].

In the interleaved case, however, our numerical simulations showed that the phase never reached steady-state but rather a pseudo-steady-state that alternated between two conditions depending on the frequency of the preceding off-resonance BS pulse. As a result, the difference in phase between interleaves is not solely due to the BSS effect and therefore does not match the phase difference of the sequential ordering scheme (Fig.2). The additional phase accrued biased the estimated BSS phase (Fig.3) and therefore the B_1^+ estimates in phantom and *in vivo* experiments. We have shown that the bias depends on intrinsic tissue properties (T_1, T_2) as well as sequence parameters (TR, RF spoiling increment, amplitude of the BS pulse).

Although the biases observed here are relatively small, the effect would approximately double if these biased B_1^+ estimates were used to quantify R_1. It is well known that an uncertainty of X% in B_1^+ results in an uncertainty of 2X% in R_1 because of its dependence on the square of the B_1^+ amplitude [4]. Similarly it can be shown, via Taylor expansion to first order, that a bias of Y% in B_1^+ will propagate into the R_1 estimate with a bias of 2Y%. Hence even small errors must be accounted for if accurate R_1 estimates are to be obtained. In fact under certain conditions, such as in CSF where the T_1 and T_2 are long, the bias can reach 15% (Fig.8) when no RF spoiling is used. This would lead to a 30% bias in R_1 in these locations.

Here, we have proposed and validated a novel acquisition and processing scheme for interleaved BSS-based B_1^+ mapping that does not suffer from these biases. Crucially, multiple echoes are acquired either side of the BS pulse and a GLM framework is used to describe the phase evolution over time. The GLM models the effects of the BS pulse, B_0 inhomogeneity, eddy currents and phase offsets both common to, and specific to, the positive and negative off-resonance frequency interleaves. The bias observed with the Classic method results from the invalid assumption that the only difference between the two interleaves is the phase imparted by the BS pulse. Indeed, as demonstrated by the numerical simulations, a difference is already present before playing out the BS pulse (Fig.2 d). The use of two distinct regressors (X^+_{offset} and X^-_{offset}) in the model matrix of the GLM allows the two interleaves to differ, even prior to the BS pulse. This removes the bias in B_1^+ that would otherwise be present. Numerical simulations (Fig.3) and phantom experiments (Fig.4) confirm this, with both showing peak differences for RF spoiling increments of 0^0 (equivalent to no RF spoiling), 60^0, 120^0 and 180^0. However, the bias was lower empirically than predicted by simulation. For example, a 3.6% bias between processing methods was observed without RF spoiling whereas the numerical simulations predicted a bias of 7% for the phantom (assuming T_1 of 550ms, T_2 of 70 ms). In agreement with the numerical simulations, the proposed GLM method removed the dependence of the B_1^+ estimates on the RF spoiling increment, the TR and the acquisition mode in both phantom (Fig.5) and *in vivo* (Fig.7 and 8) experiments.

Increased variability in the measured bias was observed in phantom experiments on the Prisma scanner, particularly with an RF spoiling increment of 137^0 (Fig.5 a, yellow curve), but not predicted by simulation. A simplified experiment acquiring only an FID signal was used to investigate this phase

stability. Without RF spoiling, a constant phase was observed on both scanners (Fig.6). This was the case regardless of the protocol. However, when RF spoiling was used, unpredicted phase variation across pulses was observed on the Prisma scanner only. The specific temporal pattern depended on the RF spoiling increment but was highly reproducible across runs, between phantom and *in vivo* experiments and across Prisma scanners (data not shown). The amplitude of the effect increased at shorter TR and higher excitation flip angle. While the pattern was consistent between phantom and *in vivo* experiments, the amplitude of the effect was larger *in vivo*, likely due to the longer T_1 (> 1s *in vivo* compared to the phantom T_1 of 0.55s), and was on the same order as the amplitude of physiologically-driven variation (Fig.6 a). The reproducible phase variation introduced a phase difference between the two interleaves, resulting in a spatially-varying error in the BSS phase estimated with the Classic method (Fig.5 a). The GLM approach, however, was robust to this effect (Fig.5 b) since it allowed for a phase difference between the two acquisitions before the BS pulse. The additional phase difference introduced by this phase variation is captured by β^{+}_{offset} and β^{-}_{Offset} preventing it from affecting the accuracy of β_{BSS}. The differences observed between the two scanner platforms, which have distinct RF architectures, may be caused by the specifics of how the pulse phase is set, e.g. differential precision or digitisation errors. These observations and their dependencies are consistent with incomplete spoiling of the transverse magnetisation as a result of imperfect RF spoiling. Since the phase variation was reproducible, the sequential acquisition order was not affected by this artefact.

In theory, the GLM method could use just a single off-resonance frequency with a reduced model matrix containing only half-length regressors for X_{BSS}, $X_{\omega_{B_0}}$, $X_{Even/Odd}$ and X^{+}_{Offset}[25]. In this case, X_{BSS} would model all the phase imparted by the BS pulse, including the component depending on B_0 inhomogeneity and chemical shift. However this could be corrected with the information captured by the second regressor $X_{\omega_{B_0}}$. However, since the BSS phase is imparted only once, the BS pulse flip angle would need to be doubled to achieve the same phase-to-noise ratio. This is problematic from a SAR perspective, and the benefit of a single off-resonance frequency acquisition would be negated if the TR were also doubled to address it.

Limitations:

Given that the GLM method relies on a multi-echo sequence, additional pre-processing steps are required compared to the Classic approach. Phase unwrapping across echoes is necessary. It has been necessary to spatially unwrap the phase difference between successive echoes to deal with large phase accumulation between successive echoes, then cumulatively add these to the first echo.

In the proposed method, multiple echoes are used to estimate the BSS phase, some of the echoes may suffer from dropout and potentially introduce noise into the estimate. To minimize this effect a weighted least-square (WLS) approach had been used to estimate the parameters of the GLM, down-weighting echoes with lower magnitude.

Conventionally, the BS pulse is applied just after the excitation pulse. Here, two echoes preceded the BS pulse and the difference of the third echoes, from the different off-resonance frequency acquisitions, was used to estimate B_1^+ using the Classic method. This reduces the minimum TE (by ~4ms) and therefore lowers the SNR relative to the single-echo method. However, while this might reduce precision, it would not be expected to introduce bias.

This study focused on short TR 3D acquisitions. For 2D acquisitions, the shot-to-shot inconsistencies may be less problematic since the TR will be longer. However, the two acquisitions of one slice will be

more separated in time which may result in additional phase differences due to motion, similar to the problem affecting sequential acquisitions.

Only the commonly used Fermi shape for the BS pulse was investigated here. More efficient pulses have been proposed[16,26] and the bias observed with the Fermi pulse may not be of the same order as for other pulses (for example the dependence on the BS pulse amplitude is greater for a hard pulse).

While we have shown how to accurately estimate the BSS phase, conversion to B_1^p may still be a source of inaccuracy if any assumptions underlying Eq.4 are violated[16].

Conclusion

Interleaved acquisitions are recommended for Bloch-Siegert based B_1^+ mapping to increase robustness to motion and scanner drift. However we have shown that with the Classic estimation method, this can introduce error into the B_1^+ amplitudes. The degree of bias depends on tissue properties and sequence settings. In theory, one could use an RF spoiling increment of 90° to be immune to this error. However, hardware imperfections can also introduce spurious phase and lead to additional errors in the B_1^+ map computed with the Classic method. We have proposed and validated a multi-echo sequence design, combined with a GLM framework, to more robustly isolate the BSS-induced phase. This allows bias free, low error estimates of the B_1^+ efficiency that do not depend on tissue properties, sequence settings or reproducible hardware imperfections. Importantly, the proposed modifications do not extend acquisition time, reduce sensitivity or increase SAR. The latter is particularly important since SAR is a limiting factor at higher field strengths.

Acknowledgment

The Wellcome Centre for Human Neuroimaging is supported by core funding from Wellcome [203147/Z/16/Z].

References

1. Sacolick LI, Sun L, Vogel MW, Dixon WT, Hancu I. Fast radiofrequency flip angle calibration by Bloch–Siegert shift. Magn. Reson. Med. 2011;66:1333–1338 doi: 10.1002/mrm.22902.

2. Padormo F, Beqiri A, Hajnal JV, Malik SJ. Parallel transmission for ultrahigh-field imaging: Parallel Transmission for Ultrahigh-Field Imaging. NMR Biomed. 2016;29:1145–1161 doi: 10.1002/nbm.3313.

3. Lutti A, Dick F, Sereno MI, Weiskopf N. Using high-resolution quantitative mapping of R1 as an index of cortical myelination. NeuroImage 2014;93:176–188 doi: 10.1016/j.neuroimage.2013.06.005.

4. Lee Y, Callaghan MF, Nagy Z. Analysis of the Precision of Variable Flip Angle T1 Mapping with Emphasis on the Noise Propagated from RF Transmit Field Maps. Front. Neurosci. 2017;11 doi: 10.3389/fnins.2017.00106.

5. Sacolick LI, Wiesinger F, Hancu I, Vogel MW. B1 Mapping by Bloch-Siegert Shift. Magn. Reson. Med. Off. J. Soc. Magn. Reson. Med. Soc. Magn. Reson. Med. 2010;63:1315–1322 doi: 10.1002/mrm.22357.

6. Pohmann R, Scheffler K. A theoretical and experimental comparison of different techniques for B1 mapping at very high fields. NMR Biomed. 2013;26:265–275 doi: 10.1002/nbm.2844.

7. Carinci F, Santoro D, von Samson-Himmelstjerna F, Lindel TD, Dieringer MA, Niendorf T. Characterization of Phase-Based Methods Used for Transmission Field Uniformity Mapping: A Magnetic Resonance Study at 3.0 T and 7.0 T. PLoS ONE 2013;8 doi: 10.1371/journal.pone.0057982.

8. Lesch A, Petrovic A, Stollberger R. Robust implementation of 3D Bloch Siegert B1 mapping. In: Proc. Intl. Soc. Mag. Reson. Med. 23. Toronto; 2015.

9. Lesch A, Schlöegl M, Holler M, Bredies K, Stollberger R. Ultrafast 3D Bloch–Siegert B-mapping using variational modeling. Magn. Reson. Med. 2019;81:881–892 doi: 10.1002/mrm.27434.

10. Saranathan M, Khalighi MM, Glover GH, Pandit P, Rutt BK. Efficient bloch-siegert B1+ mapping using spiral and echo-planar readouts. Magn. Reson. Med. 2013;70:1669–1673 doi: 10.1002/mrm.24599.

11. Basse-Lüsebrink TC, Kampf T, Fischer A, et al. SAR-reduced spin-echo-based Bloch–Siegert B1+ mapping: BS-SE-BURST. Magn. Reson. Med. 2012;68:529–536 doi: 10.1002/mrm.23259.

12. Basse-Lüsebrink TC, Sturm VJF, Kampf T, Stoll G, Jakob PM. Fast CPMG-based Bloch-Siegert B1+ mapping. Magn. Reson. Med. 2012;67:405–418 doi: 10.1002/mrm.23013.

13. Sacolick LI, Lee SK, Grissom WA, Vogel MW. Fast Spin Echo Bloch-Siegert B1 Mapping. In: Proc. Intl. Soc. Mag. Reson. Med. 19. Montreal; 2011.

14. Sturm VJF, Basse-Lüsebrink TC, Kampf T, Stoll G, Jakob PM. Improved encoding strategy for CPMG-based Bloch-Siegert B mapping. Magn. Reson. Med. 2012;68:507–515 doi: 10.1002/mrm.23232.

15. Kameda H, Kudo K, Matsuda T, et al. Improvement of the repeatability of parallel transmission at 7T using interleaved acquisition in the calibration scan. J. Magn. Reson. Imaging 2018;48:94–101 doi: 10.1002/jmri.25903.

16. Duan Q, van Gelderen P, Duyn J. Improved Bloch-Siegert Based B1 Mapping by Reducing Off-Resonance Shift. NMR Biomed. 2013;26:1070–1078 doi: 10.1002/nbm.2920.

17. Bernstein MA, King KF, Zhou XJ. Handbook of MRI Pulse Sequences.; 2004. doi: 10.1016/B978-0-12-092861-3.X5000-6.

18. Hansen MS, Sørensen TS. Gadgetron: an open source framework for medical image reconstruction. Magn. Reson. Med. 2013;69:1768–1776 doi: 10.1002/mrm.24389.

19. Walsh DO, Gmitro AF, Marcellin MW. Adaptive reconstruction of phased array MR imagery. Magn. Reson. Med. 2000;43:682–690 doi: 10.1002/(SICI)1522-2594(200005)43:5<682::AID-MRM10>3.0.CO;2-G.

20. Abdul-Rahman HS, Gdeisat MA, Burton DR, Lalor MJ, Lilley F, Moore CJ. Fast and robust three-dimensional best path phase unwrapping algorithm. Appl. Opt. 2007;46:6623–6635 doi: 10.1364/AO.46.006623.

21. Glover GH, Mueller BA, Turner JA, et al. Function Biomedical Informatics Research Network Recommendations for Prospective Multi-Center Functional Magnetic Resonance Imaging Studies. J. Magn. Reson. Imaging 2012;36:39–54 doi: 10.1002/jmri.23572.

22. Lee Y, Callaghan MF, Acosta-Cabronero J, Lutti A, Nagy Z. Establishing intra- and inter-vendor reproducibility of T1 relaxation time measurements with 3T MRI. Magn. Reson. Med. 2019;81:454–465 doi: 10.1002/mrm.27421.

23. Park DJ, Bangerter NK, Javed A, Kaggie J, Khalighi MM, Morrell GR. A Statistical Analysis of the Bloch-Siegert B1 Mapping Technique. Phys. Med. Biol. 2013;58 doi: 10.1088/0031-9155/58/16/5673.

24. Weingärtner S, Zimmer F, Metzger GJ, Uğurbil K, Van de Moortele P-F, Akçakaya M. Motion-Robust Cardiac B1+ Mapping at 3T using Interleaved Bloch-Siegert Shifts. Magn. Reson. Med. 2017;78:670–677 doi: 10.1002/mrm.26395.

25. Corbin N, Acosta-Cabronero J, Weiskopf N, Callaghan MF. Rapid B1 mapping based on the Bloch-Siegert shift using a single offset frequency and multi-echo readout. In: Proc. Intl. Soc. Mag. Reson. Med. 26. Paris; 2018.

26. Khalighi MM, Rutt BK, Kerr AB. Adiabatic RF pulse design for Bloch-Siegert B mapping. Magn. Reson. Med. 2013;70:829–835 doi: 10.1002/mrm.24507.

Supplementary Information 1

In a static magnetic field, B_0, the precessional frequency is the Larmor frequency given by $\omega_0 = \gamma B_0$. The BSS approach applies an off-resonance RF pulse with a rotating frequency of ω_2, such that $\omega_{off} = \omega_0 - \omega_2 \neq 0$. The off-resonance pulse (termed the BS pulse) modifies the precessional frequency during the time of its application. It has an amplitude B_1 such that $\omega_1 = \gamma B_1$.

In the frame of reference rotating at ω_0, the precessional frequency during this pulse changes to:

$$\omega^{rot} = \sqrt{\omega_{off}^2 + \omega_1^2} - \omega_{off} = \omega_{off}\left(\sqrt{1 + \frac{\omega_1^2}{\omega_{off}^2}} - 1\right) \quad \text{(SI1.1)}$$

If the off-resonance frequency of the BS pulse is much larger than its strength in frequency units, i.e. $\omega_{off} \gg \omega_1$, the expression reduces to:

$$\omega^{rot} = \frac{\omega_1^2}{2\omega_{off}} \quad \text{(SI1.2)}$$

Given that the precessional frequency is no longer equal to ω_0 during the BS pulse, an additional phase is accumulated. Since it is proportional to ω_1^2 this phase can be used to map the spatial distribution of B_1^+.

Allowing for local B_0 inhomogeneity, the local precessional frequency will be $\omega_0 + \Delta\omega_{B_0}$. In the rotating frame of reference and under the similar condition as before, $(\omega_{off} + \Delta\omega_{B_0}) \gg \omega_1$, the precessional frequency ω^{rot} during the BS pulse becomes:

$$\omega^{rot} = \sqrt{\left(\omega_{off} + \Delta\omega_{B_0}\right)^2 + \omega_1^2} - \omega_{off} \quad \text{(SI1.3)}$$

$$= \left(\omega_{off} + \Delta\omega_{B_0}\right)\sqrt{1 + \frac{\omega_1^2}{\left(\omega_{off} + \Delta\omega_{B_0}\right)^2}} - \omega_{off} \quad \text{(SI1.4)}$$

$$= \frac{\omega_1^2}{2\left(\omega_{off} + \Delta\omega_{B_0}\right)} + \Delta\omega_{B_0} \quad \text{(SI1.5)}$$

The first term on the right hand side of this expression, representing the frequency shift due to the BS pulse, will be called ω_{BSS}. Note that this effect adds to the phase accrued due to local B_0 inhomogeneity. The phase specifically accumulated due to the BS pulse, of arbitrary shape and duration T, is given by:

$$\phi_{BSS} = \int_0^T \omega_{BSS}\, dt \;=\; \int_0^T \frac{\omega_1^2}{2\left(\omega_{off} + \Delta\omega_{B_0}\right)} \qquad \text{(SI1.6)}$$

$$= \int_0^T \frac{\left(\gamma B_1(t)\right)^2}{2\left(\omega_{off} + \Delta\omega_{B_0}\right)} dt = \left(B_1^p\right)^2 \int_0^T \frac{\left(\gamma\, B_1^{norm}(t)\right)^2}{2\left(\omega_{off} + \Delta\omega_{B_0}\right)}\, dt$$

$B_1(t) = B_1^p * B_1^{norm}(t)$, where B_1^p is the peak amplitude of the BS pulse, and B_1^{norm} is its normalized shape. Assuming $|\Delta\omega_{B_0}| \ll |\omega_{off}|$, the first order Taylor expansion of this expression is:

$$\Phi_{BSS} = \left(B_1^p\right)^2 \int_0^T \left(\gamma\, B_1^{norm}(t)\right)^2 * \left(\left[\frac{1}{2\omega_{off}} - \frac{\Delta\omega_{B_0}}{2\omega_{off}^2}\right] + O\left(\Delta\omega_{B_0}^2\right)\right) dt \qquad \text{(SI1.7)}$$

Supplementary Information 2

Numerical simulations were carried out to evaluate the phase difference between two acquisitions with opposite off-resonance frequencies both before and after the BS pulse. A typical gradient echo acquisition was simulated in MATLAB (The MathWorks, Inc., Natick, MA) by a series of matrix operations as described below:

1- The magnetization $M = [m_x\ m_y\ m_z]^T$ of a spin ensemble is subject to a rotation by the excitation flip angle α about an axis defined by the phase ϕ of the excitation pulse.
2- During a subsequent delay TE, longitudinal and transverse relaxation were simulated with time constants T_1 and T_2, respectively. The phase at time TE is termed ϕ^{+}_{Before} if the off-resonance frequency of the upcoming BS pulse is positive, or ϕ^{-}_{Before} if the off-resonance frequency of the upcoming BS pulse is negative.
3- The application of a crusher gradient rotates the magnetization vector around the z-axis by an angle Ω_1.
4- The BS pulse, in this work a Fermi pulse described by $B_1(t) = \frac{B_1^p e^{i\omega_{off}t}}{1+\exp\left(\frac{|t|-t_0}{a}\right)}$, was then simulated as a series of small rotations indexed by $k \in [1{:}K]$. Each small rotation k is a rotation of an angle $|B_1(k * dt)| * dt$ about an axis defined by an azimuthal angle of $k * dt * \omega_{off} + \phi$.
5- A rotation of the resulting magnetization vector about the z-axis by an angle $-\Omega_1$ is then applied to simulate the crusher of opposite polarity. The resulting phase at this time is called ϕ^{+}_{After} if the frequency of the preceding BS pulse was positive, or ϕ^{-}_{After} if the frequency was negative. For simplicity, the pulse and crushers were assumed to be instantaneous from a relaxation standpoint such that Φ_{After} and Φ_{Before} have the same TE. Note that the relaxation is instead accounted for in step 7.
6- Following the second crusher gradient, a spoiler gradient was applied such that the magnetization vector from step 5 was rotated around the z-axis by an angle of Ω_2.
7- T_1 and T_2 relaxation were then simulated for the remainder of the TR period, i.e. TR-TE.
8- When RF spoiling was simulated, the phase of the RF pulses, ϕ, was incremented such that $\phi = \phi + \phi_{inc}$ and $\phi_{inc} = \phi_{inc} + \phi_{BaseInc}$.

These steps were repeated N_{exc} times, by updating the magnetization of Step 1 with the magnetization vector resulting from Step 7.

The simulation was performed for a 2D grid of spin ensembles ($N_{spin} * N_{spin}$) with varying values for Ω_1 and Ω_2 ranging from 0° to Ω_1^{max} and Ω_2^{max}, respectively. The values of the crusher dephasing Ω_1 varied along one dimension of the grid, whereas the values of the spoiler dephasing Ω_2 varied in the other direction to simulate crushers and spoiler along orthogonal axes. The integral of these spins gave the magnetisation in a single voxel.

For interleaved ordering, the sign of ω_{off} was switched before each BS pulse. For sequential ordering the sign was only switched after half the total number of pulses $\left(\frac{N_{exc}}{2}\right)$. If RF spoiling was included in the simulation, the RF spoiling phase (ϕ and ϕ_{Inc}) were reset to 0 when the sign of ω_{off} was switched in the sequential case. In the case of an interleaved acquisition, the phase increment occurred for each repetition, including when the off-resonance frequency also changes.

The Matlab code is available here: https://github.com/fil-physics/Publication-Code/tree/master/Bloch-Siegert.

The numerical values of the parameters used in the simulations are listed in Table SI2.1.

$\boldsymbol{T_1}$	Longitudinal relaxation time	[550, 1350] ms
$\boldsymbol{T_2}$	Transverse relaxation time	[70,100] ms
$\boldsymbol{TR}$	Repetition time	[30, 100] ms
$\boldsymbol{TE}$	Echo time for Φ_{Before} and ϕ_{After}	2 ms
$\boldsymbol{\alpha}$	Excitation flip angle	20°
$\boldsymbol{\omega_{off}}$	BS pulse off-resonance frequency	2 kHz
$\boldsymbol{B_1}$	BS pulse amplitude	[8, 11] μT
$\boldsymbol{T}$	BS pulse duration	2 ms
$\boldsymbol{\phi_{BaseInc}}$	RF spoiling increment	[0 50 137] ° (Figure 2) [0:10:180] ° (Figure 3)
$\boldsymbol{\Omega_1^{max}}$	Crusher gradient dephasing moment	8 π
$\boldsymbol{\Omega_2^{max}}$	Spoiler gradient dephasing moment	4 π
$\boldsymbol{N_{spin}}$	Number of spins in ensemble along each dimension	100
$\boldsymbol{N_{exc}}$	Number of excitation pulses simulated	300
$\boldsymbol{a}$	Fermi pulse parameter	0.16 ms
$\boldsymbol{t_0}$	Fermi pulse parameter	3 ms

Table SI2.2: Parameters used in the numerical simulations

The BS phase estimated by the Classic approach is simulated as:

$$\Phi_{BSS}^{Classic} = \frac{\Phi_{After}^{+} - \Phi_{After}^{-}}{2} \qquad \text{(SI2.1)}$$

The BS phase estimated by the GLM approach is simulated as:

$$\Phi_{BSS}^{GLM} = \frac{\left(\Phi_{After}^{+} - \Phi_{Before}^{+}\right) - \left(\Phi_{After}^{-} - \Phi_{Before}^{-}\right)}{2} \qquad \text{(SI2.2)}$$